

NPLIC: A Machine Learning Approach to Piecewise Linear Interface Construction

M. Ataei^a, M. Bussmann^{a,*}, V. Shaayegan^a, F. Costa^b, S. Han^c, C. B. Park^a

^a*Department of Mechanical Engineering, University of Toronto, 5 King's College Rd, Toronto, ON M5S 3G8, Canada*

^b*Autodesk, Inc., 259-261 Colchester Rd., Kilsyth, VIC. 3137, Australia*

^c*Autodesk, Inc. 2353 North Triphammer Rd., Ithaca, NY 14850, USA*

Abstract

Volume of fluid (VOF) methods are extensively used to track fluid interfaces in numerical simulations, and many VOF algorithms require that the interface be reconstructed geometrically. For this purpose, the Piecewise Linear Interface Construction (PLIC) technique is most frequently used, which for reasons of geometric complexity can be slow and difficult to implement. Here, we propose an alternative neural network based method called NPLIC to perform PLIC calculations. The model is trained on a large synthetic dataset of PLIC solutions for square, cubic, triangular, and tetrahedral meshes. We show that this data-driven approach results in accurate calculations at a fraction of the usual computational cost.

Keywords: Machine Learning, Neural Networks, PLIC, Piecewise Linear Interface Construction, Volume Of Fluid, VOF, Computational Fluid Dynamics

1. Introduction

In the numerical simulation of multiphase flows, the volume of fluid (VOF) method is widely used to track fluid interfaces through a computational domain (e.g. [1–7]). In this method, a scalar field α denotes the volume fraction of one fluid within each cell. In the case of a liquid-gas system, for example, $\alpha = 1$ in liquid cells, $\alpha = 0$ in gas cells, and $0 < \alpha < 1$ in interface cells.

Reconstruction of the interface geometry from the α field is an important step for calculating volume fluxes advected across cell boundaries. Since the pioneering work of Youngs [8], Piecewise Linear Interface Construction (PLIC) has been widely employed to geometrically reconstruct interfaces in VOF simulations.

*Corresponding author

Given a known interface normal \vec{n} and the volume fraction α_0 of an interface cell, PLIC calculates the constant C of the plane $\vec{n} \cdot \vec{x} + C = 0$ ($\vec{x} \in R^2$ in 2D or R^3 in 3D) that splits the cell into two parts, with volume fractions α_0 and $1 - \alpha_0$ (see Fig. 1). The reconstructed interface is the polygon resulting from the plane's intersection with the cell.

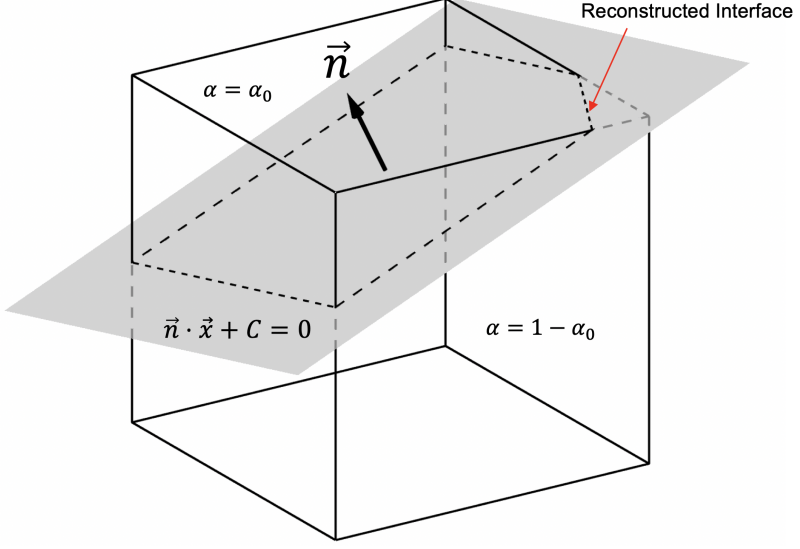


Figure 1: A plane representing the interface splits the cell into two parts, with volume fractions α_0 and $1 - \alpha_0$.

Especially in 3D, finding C involves complex geometrical operations that can be slow to compute. In some algorithms, C is found iteratively [9, 10], until the target volume fractions α_0 and $1 - \alpha_0$ are achieved within a given tolerance. For simpler geometries such as triangular or rectangular meshes, analytical solutions have been developed that reduce the computational cost [11, 12], although these approaches may also include a slow iterative step used to select one from a set of several governing equations.

Machine learning algorithms are increasingly being applied in computational science [13] and Computational Fluid Dynamics (CFD) simulations in various ways; for example, flow approximation [14–16], shape optimization for fluid flow processes [17], cardiovascular flow modeling [18], shock detection [19], computing interface curvature [20, 21], and for turbulence modeling [22–24]. In this work, we will demonstrate a machine learning approach to find C , by using artificial neural networks to relate C , α , \vec{n} , and the cell geometry. We will show that neural networks outperform both analytical and iterative PLIC algorithms, while being nearly as accurate. We limit the results of this paper to square, cubic, triangular, and tetrahedral mesh structures,

although the same methodology could be applied to other mesh types.

2. Model

2.1. Neural Network Structure

Artificial neural networks can be thought of as universal approximators capable of extracting nonlinear relationships between different parameters through a kind of machine perception [25]. Fig. 2 shows a multilayer perceptron (MLP) “fully-connected” neural network that consists of an interconnected network of so-called artificial neurons, comprised of an input layer, a series of fully-connected hidden layers, and an output layer. As shown in Fig. 3, each neuron is made up of a set of inputs x , weights w , a bias b , and output y ; the bias is added to the combined sum of input-weight products, and the result passes through an activation unit a , which is usually a sigmoid or ReLU function. In this work, we use two hidden layers each containing N neurons, and ReLU as the activation function [26], except for the output layer which is a linear function to allow for negative outputs.

Initially, the network weights and biases are ignorant of the inputs and outputs. The goal is to find a combination of weights and biases that best map the appropriate inputs to the correct PLIC solution. For this reason, the network is fed with a synthetic dataset of PLIC solutions, and the weights and biases are updated iteratively by using the gradient of the following loss function:

$$Loss(C, \bar{C}) = \sum_{batch} (C - \bar{C})^2 \quad (1)$$

which is the squared sum of the difference between each predicted value C and the actual value \bar{C} , summed over the training batch. We use four separate fully-connected neural networks to find the PLIC constants C for square, cubic, triangular, and tetrahedral meshes. The output layer of each of these networks is a single neuron outputting a constant C ; the inputs differ depending on the mesh structure.

For square and cubic meshes, the geometries are constant, and so C can be defined as only a function of the interface cell normal \vec{n} , and volume fraction α_0 . As such, for square and cubic meshes the input layers are (α_0, n_x, n_y) and $(\alpha_0, n_x, n_y, n_z)$ respectively, where n_x , n_y , and n_z are the normal vector components in a coordinate system whose axes are aligned with the cell sides. In VOF models, the interface normal

\vec{n} is often obtained from the gradient of the volume fraction field or a smoothed representation of it (e.g., $\vec{n} = \nabla\alpha/|\alpha|$) [27].

Triangular meshes are made up of arbitrarily-shaped (irregular) triangular cells, which means that the input layer must also contain geometry data. Assume that the geometry of a triangular cell is represented by three coordinate points P_1 , P_2 , and P_3 , where the edge $P_1 - P_2$ is the longest. We can minimize the amount of information representing this triangle by linearly mapping this cell into a new coordinate system $x' - y'$, such that the edge $P_1' - P_2'$ is on the x' axis from 0 to 1; i.e., $P_1' = (0, 0)$ and $P_2' = (1, 0)$, see Fig. 4. Because the edge $P_1' - P_2'$ is the longest, for any irregular triangle P_3' is limited to the area Z shown in Fig. 4, if the triangle is oriented in the positive direction. Through this normalization, the geometry of the triangle can be represented only by $P_3' = (p_x', p_y')$, and thus the input layer of the network is $(p_x', p_y', n_x', n_y', \alpha_0)$, where n_x' and n_y' are the normal vector components in the $x' - y'$ coordinate system.

As shown in Fig. 5, the geometry of the tetrahedral mesh cell can be expressed by coordinate information of the vertex $P_3' = (P_{3x}', P_{3y}', 0)$ and the vertex $P_4' = (P_{4x}', P_{4y}', P_{4z}')$, after mapping the longest edge onto the x' axis from 0 to 1. If the tetrahedral is oriented as shown in Fig. 5, both P_3' and P_4' are limited to the volume Z . The new normalized tetrahedral mesh is thus represented as a triangle cell in the $x' - y'$ plane by P_3' , while the the height of the tetrahedral is represented by P_4' . Input layer to the neural network is then $(P_{3x}', P_{3y}', P_{4x}', P_{4y}', P_{4z}', \alpha_0, n_x', n_y', n_z')$.

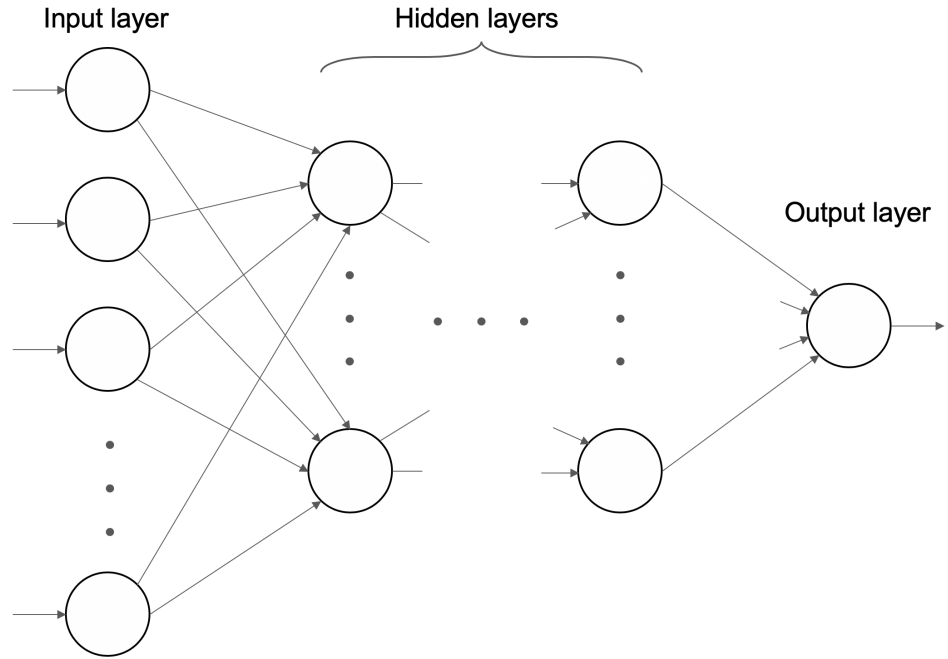


Figure 2: Architecture of a fully-connected neural network where each neuron is connected to every neuron in the previous layer.

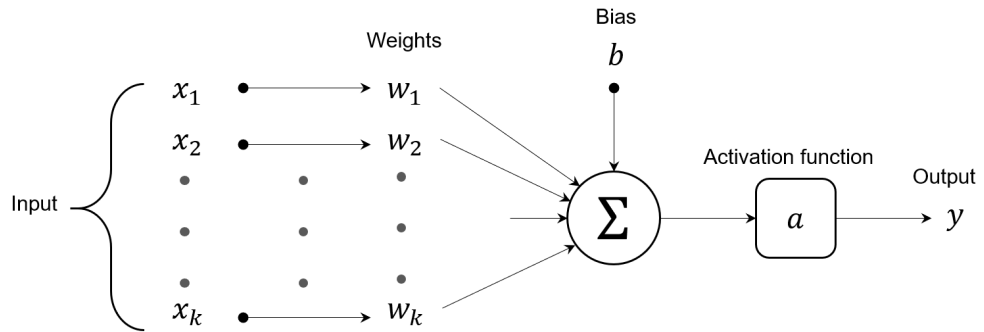


Figure 3: The structure of an artificial neuron consists of a set of inputs, weights, biases, and output.

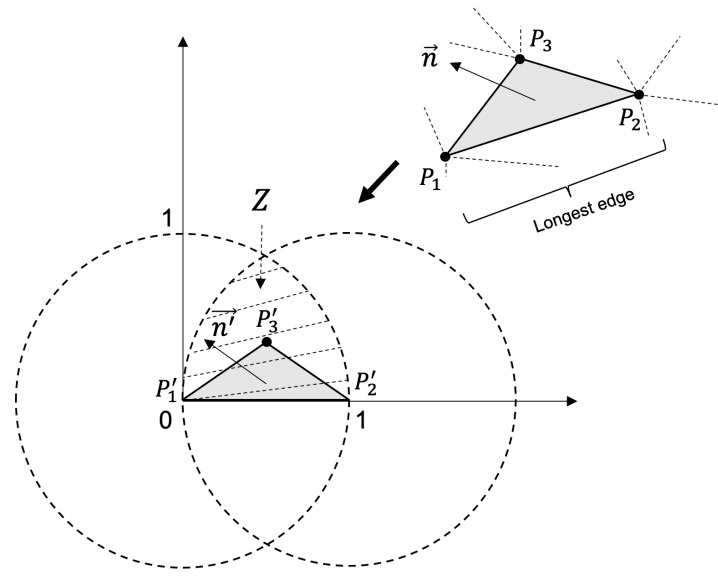


Figure 4: Normalizing a triangular cell.

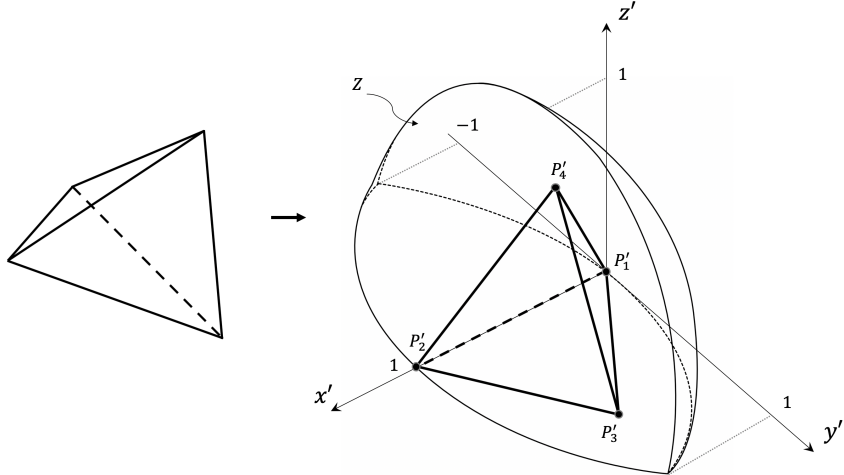


Figure 5: Normalizing a tetrahedral cell.

2.2. Generating a Synthetic Dataset

We generated synthetic PLIC datasets for each mesh type by computing the PLIC solution (i.e., the constant C) for millions of input parameters. Table 1 shows the number of samples for each input parameter. Each dataset was randomly split into three parts: 70% for training, 20% for testing, and 10% for validation. Each model was initially trained on the training dataset; during training, the validation dataset was used to prevent over-fitting; and the test dataset was used to evaluate the predictive performance of the final trained

model.

The accuracy of the machine learning PLIC depends on the degree of accuracy of the generated target output, e.g., the machine learning PLIC will theoretically achieve second-order accuracy if the algorithm used for generating the target outputs is second-order accurate. In this paper, all the target outputs in the synthetic dataset were second-order accurate.

Table 1: Number of samples of each parameter in the synthetic data generation.

Mesh type	\vec{n}	α_0	P_3'	P_4'	Training	Test	Validation	Total
Square	10^4	10^2	N/A	N/A	7×10^5	2×10^5	1×10^5	1×10^6
Cubic	10^4	10^2	N/A	N/A	7×10^5	2×10^5	1×10^5	1×10^6
Triangular	360	50	200	N/A	2.52×10^6	7.2×10^5	3.6×10^5	3.6×10^6
Tetrahedral	100	25	52	66	6.0×10^6	1.7×10^6	8.58×10^5	8.58×10^6

3. Results and Discussion

3.1. Training

The three models were developed and trained using the Google “Tensorflow” deep learning library. Computations were carried out on an NVIDIA[®] 1080 Ti Graphics Card with 11GB GDDR5X frame buffer, using a PC running Linux Ubuntu 18.1 with Intel[®] Core i7-8700K Processor (6 Cores, up to 4.7 GHz) and 32GB of DDR4 RAM.

Each neural network was trained for 500 epochs with a batch size of 128, using $N = 20$ or $N = 100$ in the hidden layer. For training, the Adam optimization algorithm [28] was used with a learning rate of 10^{-3} , and with update parameters $\beta_1 = 0.9$ and $\beta_2 = 0.999$. The training of each network took 3-4 hours. (The training time could be reduced significantly, to just a few minutes, if a much larger batch size was used (e.g., a batch size of 1024); however, we achieved a better accuracy when using a batch size of 128.)

The training performance was evaluated using the Mean Absolute Error (MAE). Fig. 6 shows MAE of the training dataset after each epoch. We observe that increasing the number of neurons in the hidden layers improves MAE, and after ~ 300 epochs MAE is almost constant.

The neural network models for computing PLIC calculations are hereafter referred to as NPLIC.

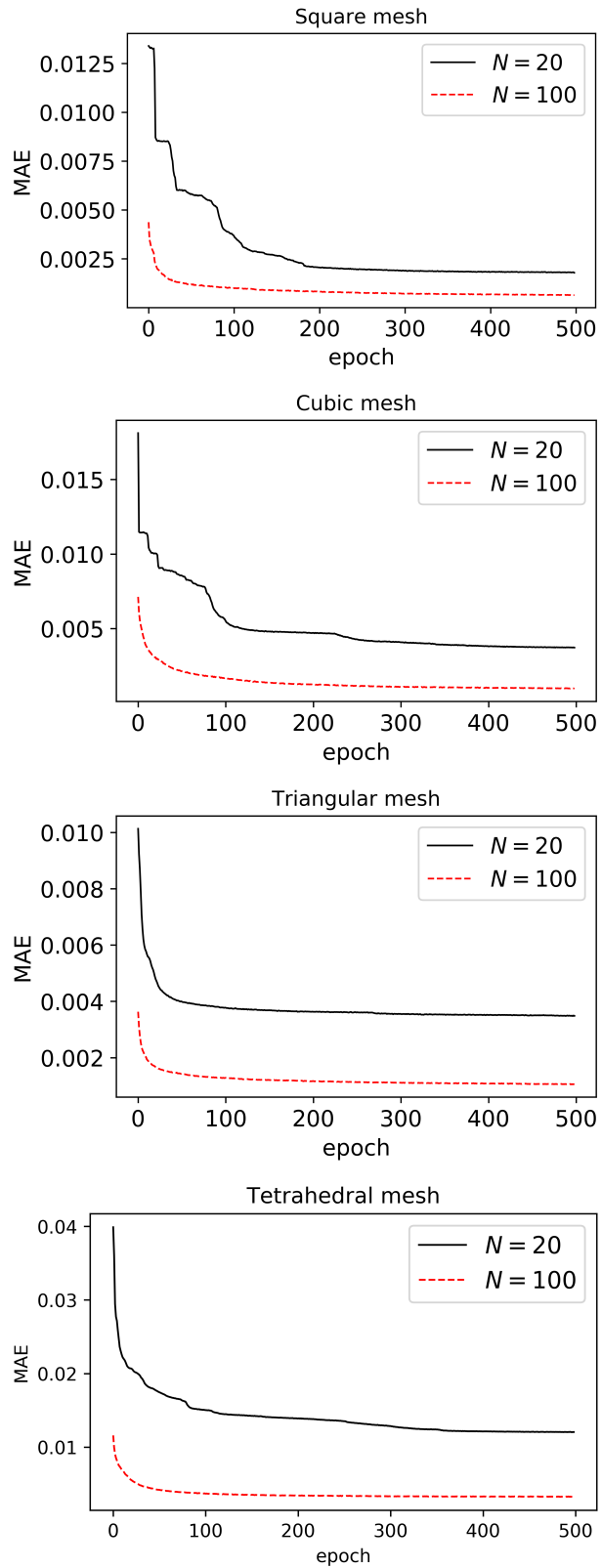


Figure 6: Mean Absolute Error (MAE) vs epoch for each mesh type.

3.2. Predictive Performance

The test dataset was used to evaluate the predictive capability of each trained model. In Fig. 7, the value of C computed by NPLIC is plotted against C from the test dataset. For a perfect fit, all the points would lie on the 45° line. It can be observed that the values of C predicted by NPLIC are in very good agreement with the test results for all four mesh types. In fact, the error for most test dataset points is close to zero. The final MAE for each trained model (based on the whole test dataset) is listed in Table 2. All models with $N = 100$, except for the tetrahedral mesh type, have an average error of less than 0.01%, which implies that NPLIC can be used in place of PLIC algorithms with little to no effect on accuracy. As the mesh complexity increases, predictably the accuracy of NPLIC decreases. For the tetrahedral mesh, with $N = 20$, MAE is as high as 1%, but by increasing the number of neurons to $N = 100$, the accuracy increases by a factor of three.

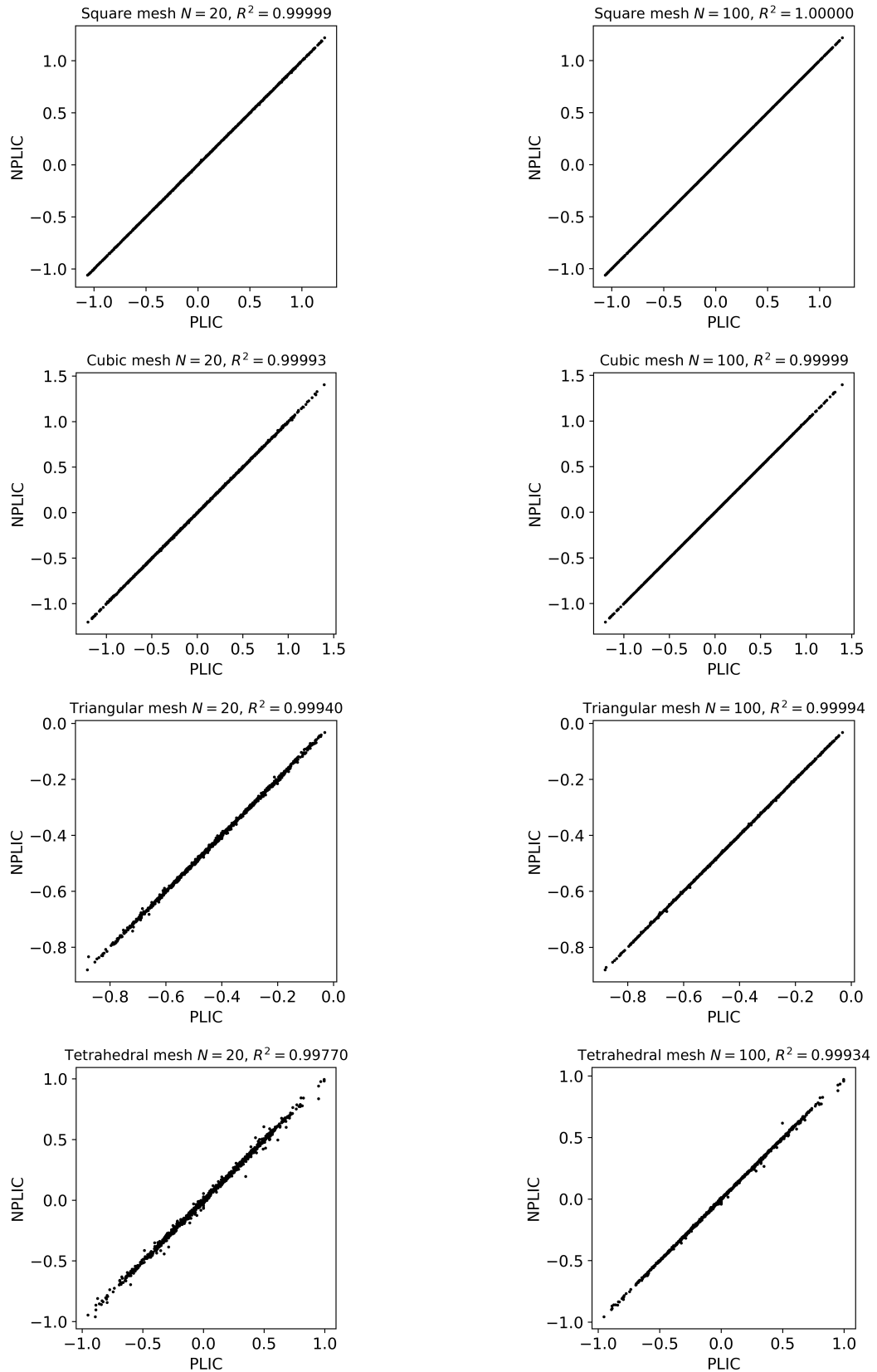


Figure 7: Plots of the NPLIC predictions vs the test data for each mesh. Note that only a thousand data points are plotted to avoid clutter.

Mesh type	MAE ($N = 20$)	MAE ($N = 100$)
Square	0.016%	0.004%
Cubic	0.021%	0.005%
Triangular	0.029%	0.010%
Tetrahedral	1.02%	0.33%

Table 2: % error of NPLIC evaluated using each whole test dataset.

3.3. Speedup

Table (3) shows a comparison of NPLIC computational cost versus a number of popular analytical and iterative PLIC models. To compare the speedups, each model was executed over the test sets using a single-core CPU. For square and cubic meshes, we compared NPLIC with the analytical PLIC model of Scardovelli and Zaleski [11], which is faster than iterative methods for rectangular meshes. For triangular meshes, we compared NPLIC with the efficient analytical model of López et al. [29]. And we compared NPLIC with the commonly used iterative PLIC model by Rider and Kothe [10] for the square and triangular meshes.

In comparison to the iterative PLIC methods, NPLIC is up to 245 times faster, and it can be more than 40 times faster than analytical PLIC methods. We believe NPLIC is by far the fastest PLIC calculator available.

Model	NPLIC Speedup ($N = 20$)	NPLIC Speedup ($N = 100$)
Square mesh (Scardovelli et al. [11], analytical)	7.39	7.10
Square mesh (Rider and Kothe [10], iterative)	34.0	32.7
Cubic mesh (Scardovelli et al. [11], analytical)	42.7	40.1
Triangular (López et al. [30], analytical)	42.2	36.5
Triangular (Rider and Kothe [10], iterative)	245.0	212.3
Tetrahedral (López et al. [30], analytical)	27.6	25.5

Table 3: Performance speedups of NPLIC for each mesh type, in comparison to analytical and iterative PLIC methods.

4. Sample Applications

NPLIC can be easily integrated into an existing codebase. The trained neural networks can be called as subroutines from other programs. Below, we showcase a few applications of NPLIC.

4.1. Reconstructing a VOF Scalar Field

Fig. 8 shows a 2D VOF scalar field for a circular bubble in a liquid. The gas and liquid phases correspond to $\alpha = 0$ and $\alpha = 1$, and the interface cells $0 < \alpha < 1$. A coarse 8×8 grid is chosen so that we can easily illustrate the reconstruction results.

In Fig. 9, the interface cells are reconstructed by the Scardovelli analytical PLIC and NPLIC models. The zoomed-in plot shows that the results of NPLIC and PLIC overlap.

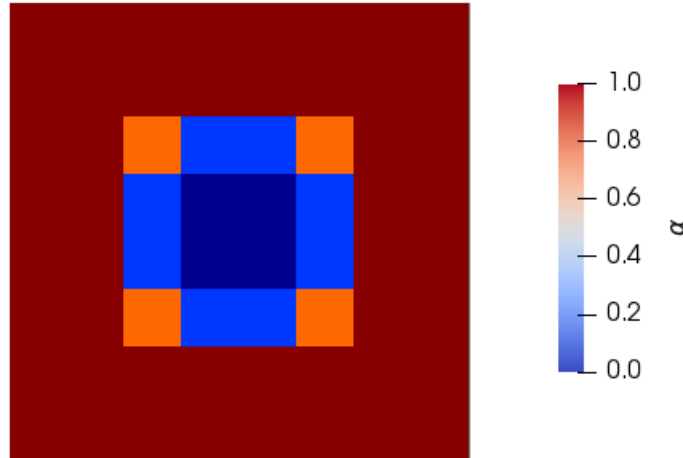


Figure 8: The α scalar field representing a circular bubble on an 8 by 8 grid.

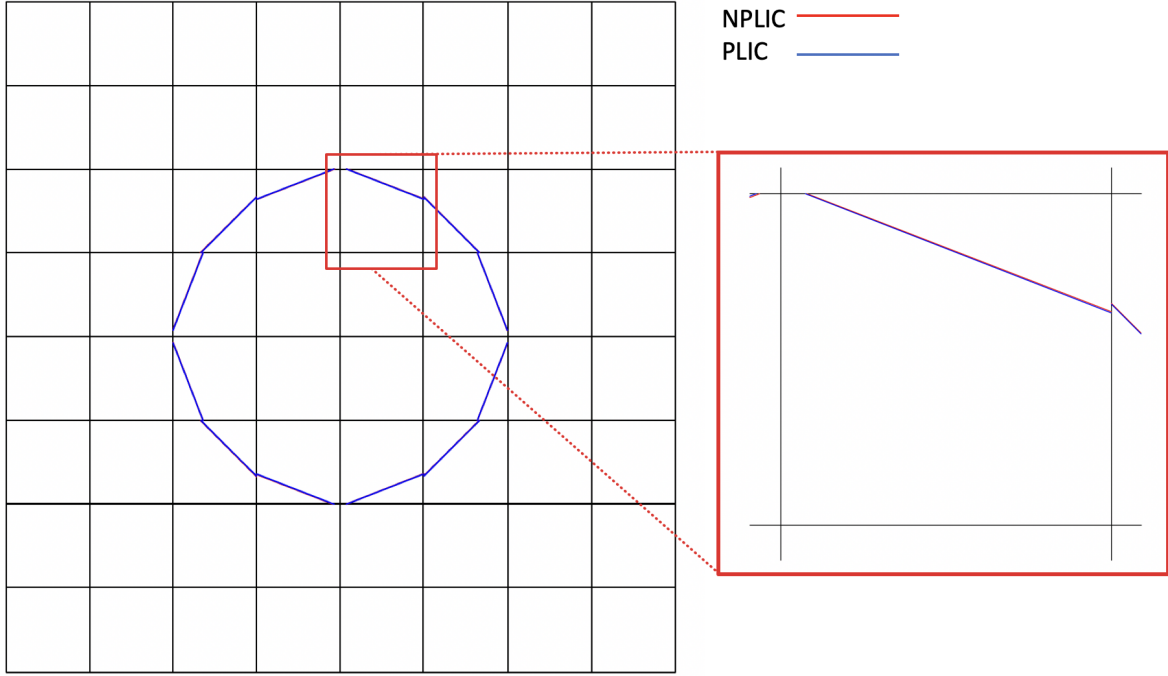


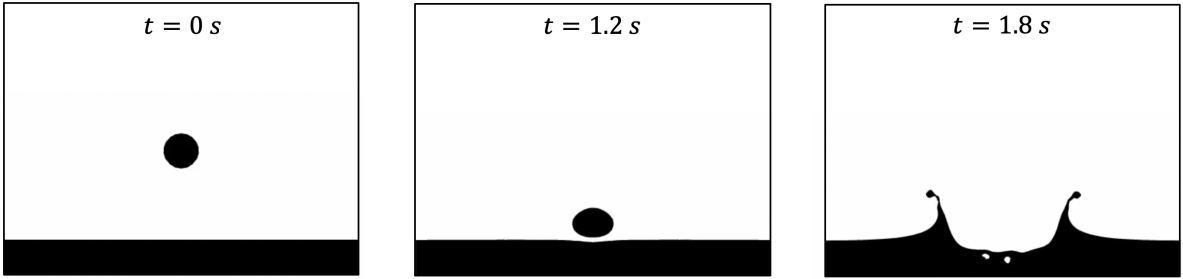
Figure 9: The NPLIC and PLIC reconstructions for the bubble interface cells.

4.2. Implementation in a CFD Solver

Basilisk (<https://basilisk.fr>) [31] is an open-source CFD solver for adaptive Cartesian meshes. Basilisk uses PLIC VOF to solve the advection equation for the volume fraction field [31, 32], by reconstructing interfaces using PLIC, and calculating volume fluxes geometrically.

We replaced the PLIC algorithm in Basilisk with NPLIC, and ran a 2D simulation of a droplet impacting a pool of liquid. As shown in Fig. 10, the NPLIC results are indistinguishable from the PLIC ones at all timesteps. In this case, NPLIC performed the interface reconstructions about five times faster.

PLIC



NPLIC

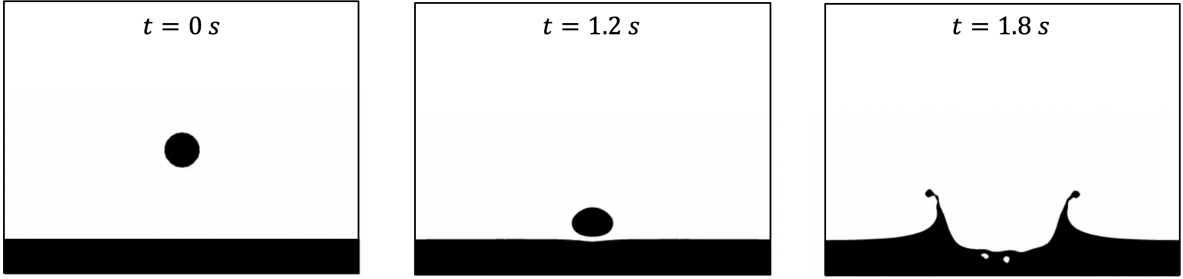


Figure 10: NPLIC performs as well as PLIC when implemented in a multiphase flow solver.

4.3. Computer Graphics

Volumetric data is commonly collected as a scalar field (for example, results of a MRI or CT scan). A surface mesh representation of the 3D data is often required for mesh-based calculations (e.g., shape optimization) or for advanced visualization. One of the most common approaches is the Marching Cube algorithm: by marching over 3D space divided into cubes, the iso-surface of the 3D data is converted into a surface mesh[33].

PLIC can also be used for visualization [34] by extracting a polyhedral mesh from a 3D iso-surface: by first translating the iso-surface into a VOF scalar field over a cubic mesh, and then by constructing the surface mesh representing the interface in each individual cube.

Figure (11) shows an iso-surface of a 3D object and the resulting surface meshes generated by PLIC and NPLIC. The surface mesh was created by NPLIC more than 30 times faster than PLIC, without any reduction in accuracy.

Admittedly, PLIC generates discontinuous surface patches, although the discontinuities are often small even on rough meshes (e.g., see Fig. 9). For mesh generation, a simple fix would be to “smooth” the surfaces by connecting them using the average of their intersection coordinates. Everything considered, NPLIC’s

simple implementation, plus substantial speedup, suggests a high potential for NPLIC as an alternative computer graphics surface mesh extraction method.

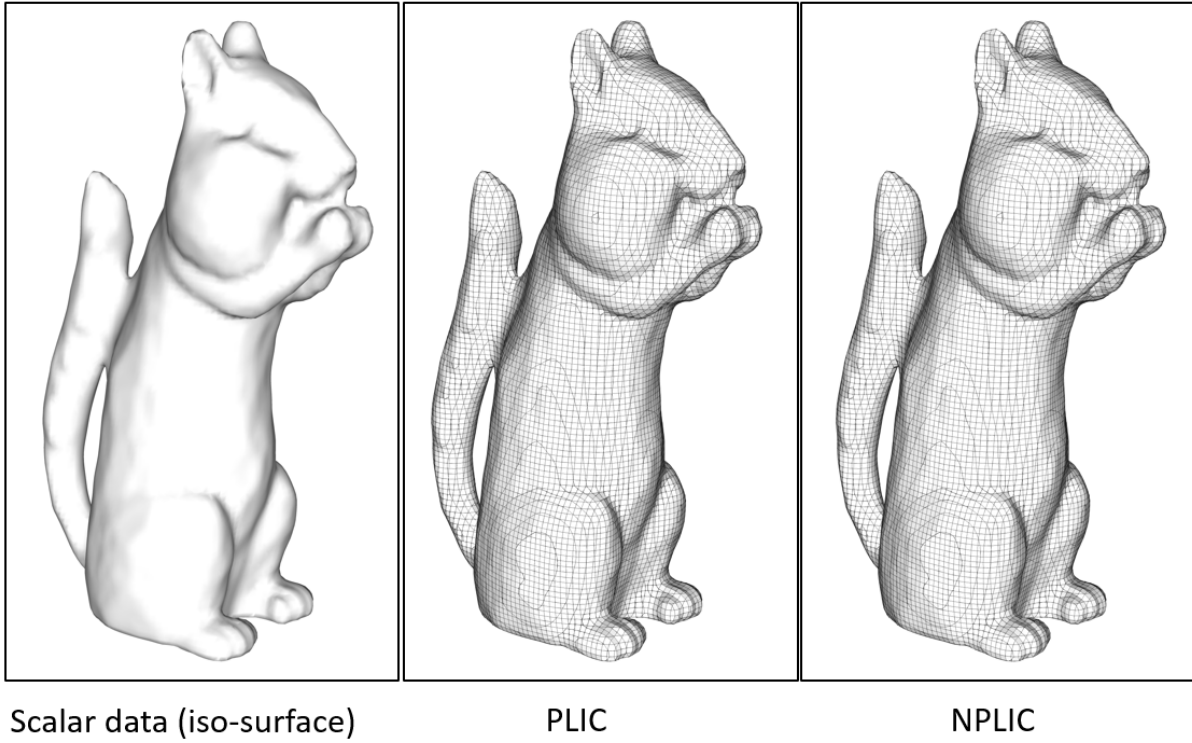


Figure 11: Iso-surface of a 3D object (left) and the polyhedral meshes extracted by PLIC (middle) and NPLIC (right). 3D object: Credit to Azorack, thingiverse.com under the Creative Commons Attribution license 3.0 Unported.

5. Conclusions

We have presented a machine learning approach to perform Piecewise Linear Interface Construction (PLIC) on square, cubic, irregular triangular, and tetrahedral meshes. Four separate fully-connected neural networks were trained on synthetic datasets. We have shown that the neural networks are capable of performing up to 245 times faster than iterative PLIC algorithms, and up to 40 times faster than analytical PLIC algorithms, with minimal loss of accuracy.

Acknowledgements

We thank the Natural Sciences and Engineering Research Council of Canada (NSERC) and Autodesk Inc. for their financial support.

References

- [1] E. Aulisa, S. Manservisi, R. Scardovelli, S. Zaleski, A geometrical area-preserving volume-of-fluid advection method, *Journal of Computational Physics* 192 (1) (2003) 355–364.
- [2] D. Gueyffier, J. Li, A. Nadim, R. Scardovelli, S. Zaleski, Volume-of-fluid interface tracking with smoothed surface stress methods for three-dimensional flows, *Journal of Computational Physics* 152 (2) (1999) 423–456.
- [3] G. Agbaglah, S. Delaux, D. Fuster, J. Hoepffner, C. Josserand, S. Popinet, P. Ray, R. Scardovelli, S. Zaleski, Parallel simulation of multiphase flows using octree adaptivity and the volume-of-fluid method, *Comptes Rendus Mcanique* 339 (2) (2011) 194–207.
- [4] M. Huang, L. Wu, B. Chen, A piecewise linear interface-capturing volume-of-fluid method based on unstructured grids, *Numerical Heat Transfer, Part B: Fundamentals* 61 (5) (2012) 412–437.
- [5] S. W. Welch, J. Wilson, A volume of fluid based method for fluid flows with phase change, *Journal of Computational Physics* 160 (2) (2000) 662–682.
- [6] K. Kleefsman, G. Fekken, A. Veldman, B. Iwanowski, B. Buchner, A volume-of-fluid based simulation method for wave impact problems, *Journal of Computational Physics* 206 (1) (2005) 363–393.
- [7] M. Renardy, Y. Renardy, J. Li, Numerical simulation of moving contact line problems using a volume-of-fluid method, *Journal of Computational Physics* 171 (1) (2001) 243–263.
- [8] D. L. Youngs, Time-dependent multi-material flow with large fluid distortion, *Numerical Methods in Fluid Dynamics* (1982) 273–486.
- [9] M. Skarysz, A. Garmory, M. Dianat, An iterative interface reconstruction method for PLIC in general convex grids as part of a coupled level set volume of fluid solver, *Journal of Computational Physics* 368 (2018) 254–276.
- [10] W. J. Rider, D. B. Kothe, Reconstructing volume tracking, *Journal of Computational Physics* 141 (2) (1998) 112–152.

[11] R. Scardovelli, S. Zaleski, Analytical relations connecting linear interfaces and volume fractions in rectangular grids, *Journal of Computational Physics* 164 (1) (2000) 228–237.

[12] X. Yang, A. J. James, Analytic relations for reconstructing piecewise linear interfaces in triangular and tetrahedral grids, *Journal of Computational Physics* 214 (1) (2006) 41–54.

[13] A. Oishi, G. Yagawa, Computational mechanics enhanced by deep learning, *Computer Methods in Applied Mechanics and Engineering* 327 (2017) 327–351.

[14] X. Guo, W. Li, F. Iorio, Convolutional neural networks for steady flow approximation, *Proceedings of the 22nd ACM SIGKDD International Conference on Knowledge Discovery and Data Mining* (2016) 481–490.

[15] F. L. Pea, V. D. Cass, A. Gosset, R. Duro, A surrogate method based on the enhancement of low fidelity computational fluid dynamics approximations by artificial neural networks, *Computers & Fluids* 58 (2012) 112 – 119.

[16] R. Swischuk, L. Mainini, B. Peherstorfer, K. Willcox, Projection-based model reduction: Formulations for physics-based machine learning, *Computers & Fluids* 179 (2019) 704 – 717.

[17] K. Hirschen, M. Schfer, Bayesian regularization neural networks for optimizing fluid flow processes, *Computer Methods in Applied Mechanics and Engineering* 195 (7) (2006) 481–500.

[18] G. Kissas, Y. Yang, E. Hwang, W. R. Witschey, J. A. Detre, P. Perdikaris, Machine learning in cardiovascular flows modeling: Predicting arterial blood pressure from non-invasive 4D flow MRI data using physics-informed neural networks, *Computer Methods in Applied Mechanics and Engineering* 358 (2020) 112623.

[19] Y. Liu, Y. Lu, Y. Wang, D. Sun, L. Deng, F. Wang, Y. Lei, A CNN-based shock detection method in flow visualization, *Computers & Fluids* 184 (2019) 1–9.

[20] Y. Qi, J. Lu, R. Scardovelli, S. Zaleski, G. Tryggvason, Computing curvature for volume of fluid methods using machine learning, *Journal of Computational Physics* 377 (2019) 155–161.

[21] H. Patel, A. Panda, J. Kuipers, E. Peters, Computing interface curvature from volume fractions: A machine learning approach, *Computers & Fluids* 193 (2019) 104263.

[22] J. Ling, A. Kurzawski, J. Templeton, Reynolds averaged turbulence modelling using deep neural networks with embedded invariance, *Journal of Fluid Mechanics* 807 (2016) 155166.

[23] F. Sarghini, G. de Felice, S. Santini, Neural networks based subgrid scale modeling in large eddy simulations, *Computers & Fluids* 32 (1) (2003) 97–108.

[24] Z. Zhou, G. He, S. Wang, G. Jin, Subgrid-scale model for large-eddy simulation of isotropic turbulent flows using an artificial neural network, *Computers & Fluids* 195 (2019) 104319.

[25] M.-C. Popescu, V. E. Balas, L. Perescu-Popescu, N. Mastorakis, Multilayer perceptron and neural networks, *WSEAS Transactions on Circuits and Systems* 8 (7) (2009) 579–588.

[26] B. Hanin, Universal function approximation by deep neural nets with bounded width and ReLU activations, *Mathematics* 7 (10) (2019) 992.

[27] D. B. Kothe, R. C. Mjolsness, RIPPLE - a new model for incompressible flows with free surfaces, *AIAA Journal* 30 (11) (1992) 2694–2700.

[28] D. P. Kingma, J. Ba, Adam: A Method for Stochastic Optimization, *arXiv e-prints* (2014) arXiv:1412.6980.

[29] J. López, J. Hernández, P. Gómez, F. Faura, VOFTools - A software package of calculation tools for volume of fluid methods using general convex grids, *Computer Physics Communications* 223 (2018) 45–54.

[30] J. López, J. Hernández, P. Gómez, F. Faura, A new volume conservation enforcement method for PLIC reconstruction in general convex grids, *Journal of Computational Physics* 316 (2016) 338–359.

[31] S. Popinet, An accurate adaptive solver for surface-tension-driven interfacial flows, *Journal of Computational Physics* 228 (16) (2009) 5838–5866.

- [32] R. Scardovelli, S. Zaleski, Direct numerical simulation of free-surface and interfacial flow, *Annual Review of Fluid Mechanics* 31 (1) (1999) 567–603.
- [33] W. E. Lorensen, H. E. Cline, Marching cubes: A high resolution 3D surface construction algorithm, *SIGGRAPH Computer Graphics* 21 (4) (1987) 163–169.
- [34] G. K. Karch, F. Sadlo, C. Meister, P. Rauschenberger, K. Eisenschmidt, B. Weigand, T. Ertl, Visualization of piecewise linear interface calculation, *2013 IEEE Pacific Visualization Symposium (PacificVis)* (2013) 121–128.